

Article

Fabrication of Effective Co-SnO₂/SGCN Photocatalysts for the Removal of Organic Pollutants and Pathogen Inactivation

Mohsin Javed ¹, Sana Iqbal ¹, Muhammad Azam Qamar ^{1,*}, Mohammad Shariq ^{2,*}, Inas A. Ahmed ³, Amal BaQais ⁴, Hanan Alzahrani ², Syed Kashif Ali ⁵, N. A. Masmali ², Talal M. Althagafi ⁶, and Mohd. Shakir Khan ⁷

¹ Department of Chemistry, School of Science, University of Management and Technology, Lahore 54770, Pakistan

² Department of Physics, College of Science, Jazan University, Jazan 45142, Saudi Arabia

³ Department of Chemistry, Faculty of Science, King Khalid University, Abha 62224, Saudi Arabia

⁴ Department of Chemistry, College of Science, Princess Nourah Bint Abdulrahman University, Riyadh 11671, Saudi Arabia

⁵ Department of Chemistry, College of Science, Jazan University, Jazan 45142, Saudi Arabia

⁶ Department of Physics, College of Science, Taif University, Taif 21944, Saudi Arabia

⁷ Department of Physics, College of Science, Al-Zulfi, Majmaah University, Al-Majmaah 11952, Saudi Arabia

* Correspondence: qamariub@gmail.com (M.A.Q.); mohammadshariq@jazanu.edu.sa (M.S.)

Abstract: Substantial improvement is needed in efficient and affordable decolorization and disinfection methods to solve the issues caused by dyes and harmful bacteria in water and wastewater. This work involves the photocatalytic degradation of methylene blue (MB) as well as gram-negative and gram-positive bacteria by cobalt-doped tin oxide (Co-SnO₂) nanoparticles (NPs) and Co-SnO₂/SGCN (sulfur-doped graphitic carbon nitride) nanocomposites (NCs) under sunlight. The coprecipitation approach was used to synthesize the photocatalysts. Maximum methylene blue (MB) photocatalytic degradation was seen with the 7% Co-SnO₂ NPs compared to other (1, 3, 5, and 9 wt.%) Co-SnO₂ NPs. The 7% Co-SnO₂ NPs were then homogenized with different amounts (10, 30, 50, and 70 weight %) of sulfur-doped graphitic carbon nitride (SGCN) to develop Co-SnO₂/SGCN heterostructures with the most significant degree of MB degradation. The synthesized samples were identified by modern characterization methods such as FT-IR, SEM, EDX, UV-visible, and XRD spectroscopies. The Co-SnO₂/50% SGCN composites showed a significant increase in MB degradation and degraded 96% of MB after 150 min of sunlight irradiation. Both gram-negative (*E. coli*) and gram-positive (*B. subtilis*) bacterial strains were subjected to antibacterial activity. All samples were shown to have vigorous antibacterial activity against gram-positive and gram-negative bacteria, but the Co-SnO₂/50% SGCN composites exhibited the maximum bactericidal action. Thus, the proposed NC is an efficient organic/inorganic photocatalyst that is recyclable and stable without lowering efficiency. Hence, Co-SnO₂/50% SGCN has the potential to be employed in water treatment as a dual-functional material that simultaneously removes organic pollutants and eradicates bacteria.

Keywords: Co-SnO₂; photocatalytic degradation; bactericidal; sunlight; composites



Citation: Javed, M.; Iqbal, S.; Qamar, M.A.; Shariq, M.; Ahmed, I.A.; BaQais, A.; Alzahrani, H.; Ali, S.K.; Masmali, N.A.; Althagafi, T.M.; et al. Fabrication of Effective Co-SnO₂/SGCN Photocatalysts for the Removal of Organic Pollutants and Pathogen Inactivation. *Crystals* **2023**, *13*, 163. <https://doi.org/10.3390/cryst13020163>

Academic Editor: Claudia Graiff

Received: 20 December 2022

Revised: 6 January 2023

Accepted: 12 January 2023

Published: 17 January 2023



Copyright: © 2023 by the authors. Licensee MDPI, Basel, Switzerland. This article is an open access article distributed under the terms and conditions of the Creative Commons Attribution (CC BY) license (<https://creativecommons.org/licenses/by/4.0/>).

1. Introduction

Human activities such as industrialization and urbanization are increasing day by day with the increase of urbanization [1]. Organic pollutants such as industrial dyes and agricultural wastes are the major causes of aquatic pollution, due to which human health and its ecosystem are affected badly [2–5]. Pharmaceutical, chemical, and textile industries dispose of organic pollutants and dyes directly into the environment and produce colored wastewater [4–7]. Textile industries are releasing about 10–50 mg/L of dye during the dyeing process which is a high enough concentration to pollute water along with colors [8]. In developing countries, 1.6 million deaths per year occur just because of

drinking contaminated, untreated water [9,10]. Methylene blue is the most commonly used synthetic cationic industrial dye and is used for silk, wood, and cotton dyeing [11–14]. Long-term exposure to methylene blue causes serious health risks in humans, including increased heart rate, eye injury, shocks, vomiting, and necrosis [14,15]. Due to their complex structure, organic pollutants are resistant to degradation by simple treatment methods [16–18].

Advanced oxidation processes (AOPs) have huge potential for treating a wide range of contaminants along with improving wastewater biodegradability [15–17]. For industrial wastewater treatment, photodegradation by photocatalysis is regarded as an advantageous technique due to its low-cost photons, lower toxicity, and lack of secondary pollution [18–23]. Heterogenous catalysis is involved in photocatalytic degradation, where sunlight is absorbed by semiconductor photocatalysts. As a result, electron-hole pairs are generated, which then interact with contaminants and give carbon dioxide and water as the final products [20,24–26].

For the degradation of organic pollutants, many types of photocatalysts are used, such as metal oxides, metal sulfides semiconductors, and nanomaterials. Among these materials, oxides (for example SnO_2 , ZnO , TiO_2 , CuO , and Fe_2O_3) are extremely important and are widely used in the degradation of pollutants and dyes [27–31]. SnO_2 have great importance and have an energy band gap of 3.5 to 3.8 eV, which falls under the UV region [32]. Tin oxide, such as titanium oxide, exhibits high photocatalytic activity due to its rutile structure [33]. It is widely used in chemical sensors, transparent electrodes, solar cells, and gas sensors because of its excellent properties [34–36]. Tin oxide (SnO_2) can be synthesized by various methods such as Hydrothermal, Coprecipitation, Sol-gel, Solvothermal, and Thermal decomposition [37–40]. Coprecipitation is a wet chemical method that is widely used for the synthesis of nanomaterials because it is an energy-efficient, simple, low-temperature technique that also provides homogeneity [41–45]. Kim et al. adopted the coprecipitation method in order to prepare tin oxide particles in the nanosize range. Synthesized SnO_2 nanoparticles were used for the photodegradation of methylene blue [46]. The co-precipitation approach for the manufacture of SnO_2 nanoparticles was demonstrated by Tazikeh et al. [47].

However, the tin oxide can be photoactivated only by UV irradiation due to its large band gap. It accounts for only 4–5% of solar radiation, leaving a significant portion of solar energy unaccounted for [48,49]. By doping tin oxide with suitable metal such as cobalt, the band gap can be reduced, which lies in the visible region [50,51]. Furthermore, n-type semiconductors used in the fabrication of S-scheme photocatalysts with an appropriate band gap can improve the optical and photocatalytic properties of the material [52,53]. Cobalt-doped tin oxide nanoparticles and sulphur-doped graphitic carbon nitride have been recommended for S-scheme Co- SnO_2 /SGCN heterojunction. In previous projects, the removal of pollutants with Co- SnO_2 [42,48], SnO_2 /r GO [54,55], TiO_2 / SnO_2 [56], g- C_3N_4 /rGO/ SnO_2 [57] has been reported.

In this project, the synthesis of tin oxide, cobalt-doped tin oxide with various percentages of cobalt (1, 3, 5, 7, and 9), and 7% Cobalt doped tin oxide composites with various percentages of sulphur doped graphitic carbon nitride (10, 30, 50, 70) were prepared by the simple and facile coprecipitation method. Photodegradation of methylene blue dye was carried out with these synthesized photocatalysts under sunlight. Both gram-negative (*E. coli*) and gram-positive (*B. subtilis*) bacterial strains were subjected to antibacterial activity.

2. Experimental

2.1. Materials

Distilled water, Cobalt nitrate hexahydrate ($\text{Co}(\text{NO}_3)_2 \cdot 6\text{H}_2\text{O}$) (purity 98%, sigma-Aldrich), Tin chloride dihydrate ($\text{SnCl}_2 \cdot 2\text{H}_2\text{O}$) (98%, sigma-Aldrich), Sodium hydroxide (NaOH) (purity 98%, sigma-Aldrich), Thiourea $\text{CH}_4 \text{N}_2\text{S}$, (AppliChem, 98% purity) Nutrient agar, Nutrient broth Microgen and MB ($\text{C}_{16}\text{H}_{18}\text{ClN}_3\text{S}$) Simpsons.

2.2. Synthesis of SnO₂ Nanoparticles

Chemical precipitation was used to produce tin oxide nanoparticles. SnCl₂·2H₂O was used as a source of tin. In this method, 5 g of tin chloride dihydrate was weighed and dissolved into 100 mL of distilled water by continuous vigorous stirring on a magnetic stirrer at room temperature for 20 to 30 min, obtaining a clear and homogeneous solution. Then a 1 M solution of NaOH was added dropwise into the solution on constant stirring until pH reached 8. On observing white precipitates, the solution was filtered with filter paper (Grade 42) and washed again and again in order to remove chloride ions until the pH was maintained at seven, which was continually checked with pH meter. After washing, the precipitates were dried in an oven at 70 °C for 24 h. After that, the precipitates were annealed in a muffle furnace at 600 °C for 3 h. The obtained tin oxide was ground with a mortar and pestle to obtain powdered tin oxide.

2.3. Synthesis of Co-SnO₂

A chemical precipitation method was used to synthesize a series of Co-doped SnO₂ by varying the cobalt percentage (1, 3, 5, 7, and 9 wt.%). For the synthesis of 1% Co-doped SnO₂, 0.063 g of cobalt nitrate hexahydrate and 4.129 g of tin chloride dihydrate were dissolved in 100 mL of distilled water on vigorous and constant stirring with the magnetic stirrer. Stirring continued until a clear and homogenous solution was obtained. The pH was then kept at seven by adding drops of a 1 M solution of NaOH to the stirring solution, resulting in the observation of white precipitates. The solution was filtered and washed again and again to remove chloride ions. The precipitates were then dried in an oven at 70 °C for 24 h. Dried precipitates were annealed for 3 h in a muffle furnace in an air atmosphere at 600 °C. The obtained material was ground in a mortar and pestle to obtain powdered cobalt-doped tin oxide nanoparticles. The same procedure was used to synthesize 3, 5, 7, and 9 wt.% cobalt-doped tin oxide nanoparticles. The amount of cobalt salt and tin salts for the composition of cobalt-doped tin oxide is mentioned in Table 1.

Table 1. Composition of Co-SnO₂ nanoparticles.

Percentage	SnCl ₂ ·2H ₂ O (g)	Co(NO ₃) ₂ ·6H ₂ O (g)
1%	4.129	0.063
3%	4.817	0.187
5%	4.712	0.315
7%	4.607	0.447
9%	4.515	0.576

2.4. Synthesis of Sulfur Doped Graphitic Carbon Nitride

Sulfur-doped graphitic carbon nitride was synthesized by the thermal polycondensation method from thiourea. For this purpose, the calculated amount of thiourea is weighed, placed in a crucible, and kept in a muffle furnace under an air atmosphere at a temperature starting from 25 °C. Heat at this temperature for half an hour at a rate of 5 °C per minute until the temperature reaches 550 °C. The yellow-colored material was obtained, which was ground into fine powder.

2.5. Synthesis of Co-SnO₂/SGCN Nanocomposites

Chemical precipitation was used to create a series of cobalt-doped tin oxide composites with sulfur-doped graphitic carbon nitride by altering the percentage of SGCN (10, 30, 50, and 70 wt.%). For this purpose, 0.27 g of sulphur-doped graphitic carbon nitride was dissolved in 100 mL of solution and sonicated for 15 min. After 15 min, this solution was put on the stirrer to add 4.600 g of SnCl₂·2H₂O to the solution of SGCN in 100 mL of water. Then, as a cobalt source, 0.447 g of cobalt nitrate hexahydrate was added to the vigorously stirring solution. It is stirred continually until a clear and homogeneous

solution is observed. To achieve pH 8, a 1 M solution of NaOH was added dropwise. When white precipitates were observed, the solution was filtered with filter paper and washed with distilled water to remove chloride ions until the pH maintained at 7. After washing, the precipitates were dried in an oven at 60 °C for 24 h. This dried material was then placed into the muffle furnace in an air atmosphere at 600 °C for 3 h. Cobalt-doped tin oxide composites with SGCN were ground to a fine powder in a mortar and pestle. The remaining percentage of composites was also prepared in the same way, and the amount of salt for each series is given in Table 2.

Table 2. Composition of Co-SnO₂/SGCN NCs.

Sr. No	% Age of SGCN in NCs	SnCl ₂ ·2H ₂ O (g)	Co(NO ₃) ₂ ·6H ₂ O (g)	Sulfur Doped Graphitic Carbon Nitride
1	10%	4.607	0.447	0.275 g
2	30%	4.607	0.447	0.827 g
3	50%	4.607	0.447	1.379 g
4	70%	4.607	0.447	1.931 g

2.6. Material Characterization

Various synthesized nanoparticles and nanocomposites were characterized by using various techniques. The crystalline structure was determined by a powder X-ray diffractometer with a scan rate of 0.2° s⁻¹ ranging from 20 to 80°. Cu K α radiation ($k = 1.54056 \text{ \AA}$) was applied at 40 kV and 30 mA. The surface morphology of synthesized materials was examined by transmission electron microscope (TEM, JEOL-JEM-1230). FTIR analysis to obtain the functional group study was carried out on FTIR spectrometer in the range of 4000–400 cm⁻¹. The photocatalytic degradation efficacy of samples was measured by a UV-visible spectrophotometer (Shimadzu 1700) with a wavelength range of 200–800 nm. The percentage of elemental composition was obtained by using energy-dispersive spectroscopy (EDS).

2.7. Photocatalytic Activity

To check the photocatalytic activity of prepared materials, methylene blue was used as a standard pollutant. The photocatalytic efficiency of pure tin oxide, doped with cobalt and composite with SCN against methylene blue was monitored via UV-Visible spectroscopy. For this purpose, 0.2 g of prepared photocatalysts was dissolved in 100 mL of methylene blue solution (0.12 g/L in distilled water) in petri dishes. After sonicating the solution for 15 min, it was placed in darkness for 30 min to reach absorption-desorption equilibrium. After that, solutions were placed under the irradiation of sunlight (68–73 klux) until they were completely degraded. Five mL of aliquots were taken from each sample after 30 min interval, and changes in the absorption band (664 nm) were recorded using the UV-Vis spectrum. This was done to look into photocatalytic activity.

2.8. Antibacterial Activity

The antibacterial activity of tin oxide, cobalt-doped tin oxide, and composites with Sulphur doped graphitic carbon nitride were studied by the agar-well diffusion method. For this purpose, strains of gram-positive (*B. subtiles*) and gram-negative (*E. coli*) were examined.

2.8.1. Preparation of Inoculum

Inoculum for both positive and negative strains was prepared separately by dissolving 0.32 g nutrient broth in 25 mL of distilled water and then stirring for 15 min. After 15 min, flasks were taken out of the autoclave and cooled to room temperature. In this solution, 2–3 drops of bacterial strains were added. Both the flasks were then placed in the shaker for 24 h.

2.8.2. Preparation of Petri Plates

First of all, Petri dishes were sterilized in an autoclave and divided into four sections with permanent markers. These sections included one blank hole and three holes for sample solutions with varying concentrations. Next, 4 g of nutrient agar and 2 g of nutrient broth were added to a flask containing 100 mL of distilled water. This mixture was sterilized in an autoclave and then boiled for 5–10 min. The mixture was poured into petri dishes, which were already prepared and kept in a laminar flow cabinet. When the mixture was cooled down, the inoculum was spread on the surface of the gel. When it was completely dry, small wells were bored with a borer in each section. Standard solutions of varying concentrations, i.e., 100 ppm, 150 ppm, 200 ppm, and 250 ppm solutions, were poured into the wells with the help of a micropipette. All the petri dishes were placed in the incubator for 24 h. Results were obtained by measuring the diameter of the zone of inhibition (ZOI), which was compared with the blank hole.

3. Results and Discussion

3.1. XRD Analysis

The crystallinity and crystalline structure of all the samples were analyzed by X-ray diffractometer at 10–80°. The diffraction patterns are given in Figure 1. The obtained pattern for SnO₂ revealed that no additional impurity peaks appeared in the pattern. It is revealed that all the diffraction peaks are according to the tetragonal rutile structure of SnO₂. The obtained pattern shows 11 peaks with 2 θ , which are due to (110), (101), (200), (211), (220), (002), (310), (112), (301), (202), (321) facets of crystals. All these diffraction peaks are correctly matched with the reported values given in ICDD 01-088-0287 and JCPDS 00-072-1147 [32]. This result shows that the pattern of 5% Co-SnO₂ exactly resembles that of pure tin oxide peaks in an XRD pattern with a decrease in peak intensity and a slight shift of the (101) peak. However, by doping cobalt and changing the lattice parameters, the average grain size is decreased. So, crystallinity increases by doping tin oxide with cobalt. This is because Co²⁺ has a smaller ionic radius (0.060 nm) than Sn⁴⁺ (0.069 nm) and has lower valence states than the host Sn⁴⁺ cations [32,58]. Figure 1 shows the XRD record for sulphur-doped graphitic carbon nitride. Two unique peaks may be detected in this pattern, at 13.02° and 27.3°, which correspond to the crystal's 100 and 002 facets, respectively. The effective synthesis of sulphur-doped graphitic carbon nitride is documented in JCPDS number 00-087-1526. Figure 1, shows the X-ray diffraction pattern of a nanocomposite of 50 percent sulphur doped graphitic carbon nitride and 7 percent cobalt-doped tin oxide (7% Co-SnO₂/50% SGCN). Various peaks can be observed in this diffractogram. The peaks at 27.4° and a minor peak at 14° are due to the presence of sulphur-doped graphitic carbon nitride in the 002 facet. The presence of Co-doped SnO₂ is confirmed by the other peaks located at (110), (101), (200), (211), (220), (002), (310), (112), (301), (202), (321). The intensity of the peaks obtained from the XRD pattern of 7% Co-SnO₂/50% SGCN was lower than that of pure SnO₂ nanoparticles and 7% cobalt-doped tin oxide nanoparticles. Moreover, peak broadening with a slight shift towards lower theta at 27.08° to 26.86° was observed which confirms the successful synthesis of the nanocomposite, which contains cobalt-doped tin oxide and 50% sulphur-doped graphitic carbon nitride. These results indicate that by inserting SGCN in cobalt-doped tin oxides nanoparticle, the growth of grain size is reduced, which provides high porosity and a large surface area. The average crystallite size calculated for SnO₂ and Co-SnO₂ using the Scherrer equation from XRD data was found to be 15 nm and 13 nm respectively.

3.2. Morphology and Elemental Composition Analysis

EDX spectrum of SnO₂, Co-SnO₂, and Co-SnO₂ composite with SGCN are shown in Figure 2a–c. The spectrum of SnO₂ (Figure 2a) and Co-SnO₂ (Figure 2b) revealed the existence of tin (Sn), oxygen (O), and cobalt (Co) elements with slightly higher atomic and weight percentages of tin. Similarly, the EDX spectrum of Co-SnO₂ composite with SGCN (Figure 2c), shows the existence of carbon (C), cobalt (Co), nitrogen (N), oxygen (O),

sulfur (S), and tin (Sn) elements. The percentage composition of these components is also given along with the elemental spectrum. Detected elements in the EDX spectrum, confirm the successful synthesis of the Co-SnO₂/SGCN composite.

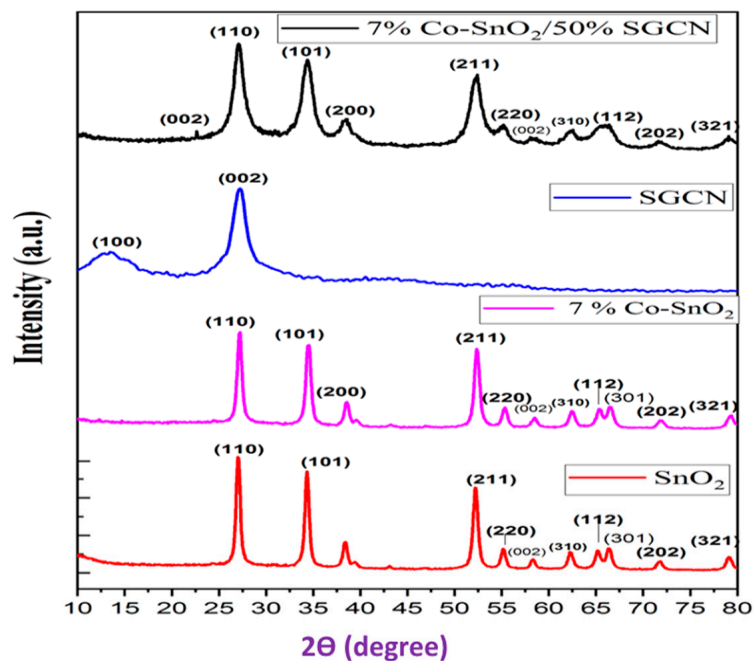


Figure 1. XRD pattern of SnO₂, 7%Co-SnO₂, SGCN, and 7%Co-SnO₂/50%SGCN.

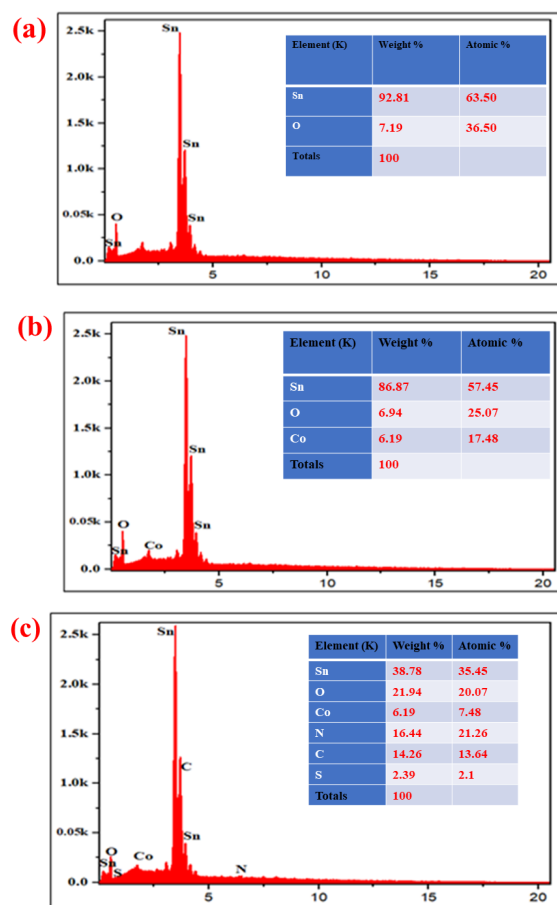


Figure 2. EDX images of SnO₂ (a), Co-SnO₂ NPs (b), and Co-SnO₂/SGCN NCs (c).

Figure 3a–c shows SEM images used to describe the morphological structure of SnO₂, Co-SnO₂ NPs, and Co-SnO₂/SGCNs. The SEM images of SnO₂ (Figure 3a) and Co-SnO₂ NPs (Figure 3b) exhibit spherical morphology with enough agglomeration. The images in Figure 3c reveal the morphology of SGCN/Co-SnO₂ NCs. These images also show a high degree of agglomeration, and the distinction between NPs and SGCN is not possible.

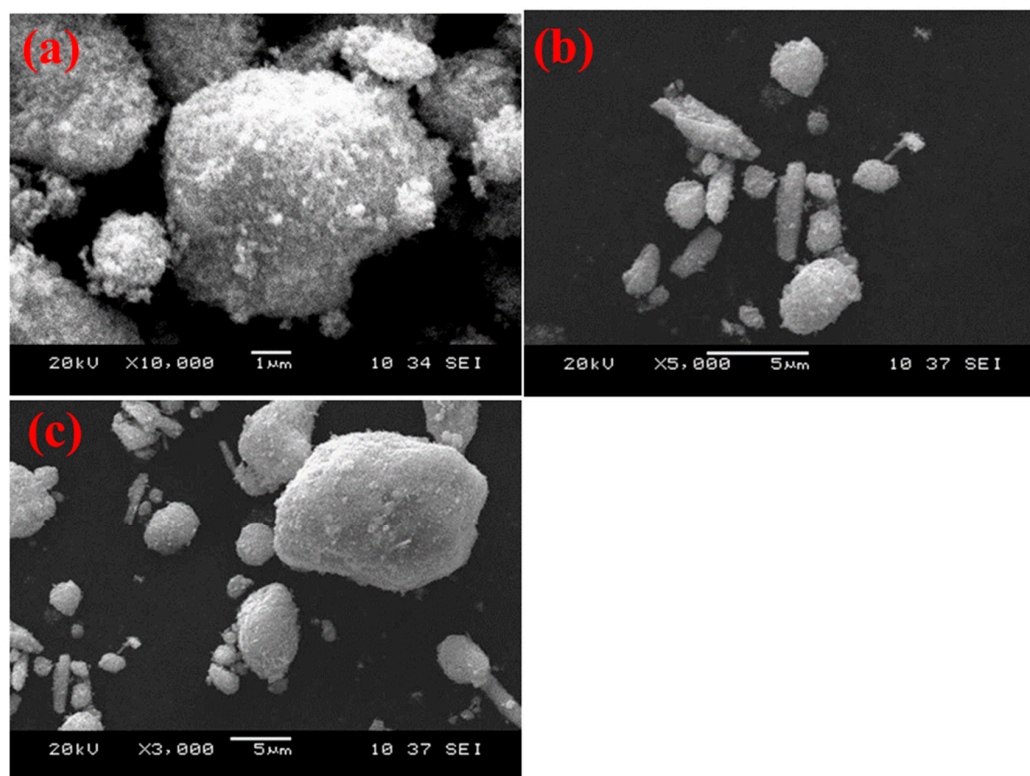


Figure 3. SEM images of SnO₂ (a), Co-SnO₂ NPs (b), and Co-SnO₂/SGCN NCs (c).

3.3. FTIR Analysis

To reveal the functional group analysis, FTIR is an important technique [59,60]. Samples of SnO₂, 7% Co-SnO₂, and 7% Co-SnO₂/50% SGCN were examined using an FTIR spectrometer in the range of 4000–400 cm^{−1}. Figure 4 represents the FTIR spectra of the above-mentioned nanomaterial.

The peak at 3300–3400 cm^{−1} is due to the O–H stretching vibration, which is most likely related to the fact that the spectrum was not captured in situ and some water adsorption from the surrounding environment occurred. Another band is observed at 1600–1700 cm^{−1}, which represents the vibrational peak of C=O. A peak at 1087 cm^{−1} has also appeared, which represents C–O bond stretching. This may occur due to the release of CO₂ during annealing in the furnace. A minor peak of Sn–OH is also observed at 1250 cm^{−1}. The peak of the O–Sn–O functional group of tin oxide is observed at about 638, 632, and 620 cm^{−1} for SnO₂, 7% Co-SnO₂, and 7% Co-SnO₂/50% SGCN respectively, which ensures the presence of crystalline phase of tin oxide. The positions, widths, and forms of IR peaks change dramatically after Co doping, showing that the Co ion has been integrated into the SnO₂ host. Furthermore, due to the modest quantity of cobalt concentration utilized, the peak position and intensity for Co-doped tin oxide barely changed. Shifting of metal–oxygen peak from 638 to 620 cm^{−1}, as well as other peaks, also shifted towards higher wavelengths and lower wavenumber. The shifting of peaks towards the lower region shows a red shift or bathochromic effect on absorbance in the visible region. These results confirm that Co ions have been substituted into the regular lattice of the SnO₂ site. Furthermore, due to the modest quantity of SGCN, the peak position and intensity for Co-doped tin oxide

nanoparticles and composites barely changed. When cobalt-doped tin oxide is attached to SGCN, it clearly indicates a red shift, which causes absorption in the visible region.

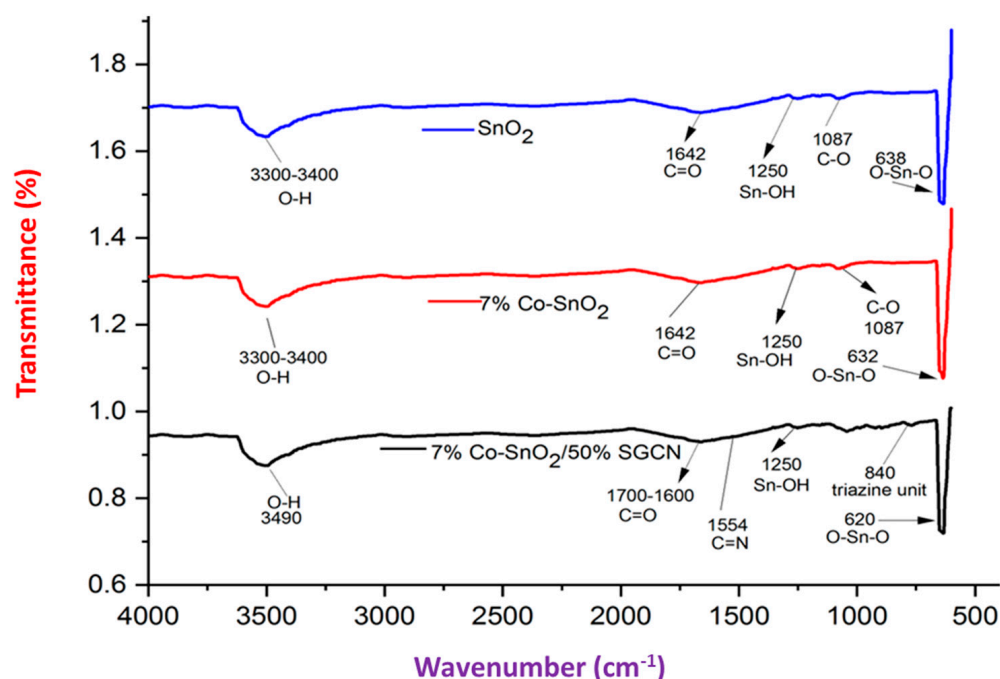


Figure 4. FTIR spectra of SnO₂, 7% Co-SnO₂ and 7% Co-SnO₂/50% SGCN.

3.4. Optical Properties

All the synthesized nanomaterials were examined using UV-visible spectroscopy, and Figure 5a shows the respective absorption spectra. While the band gap calculation of prepared samples was done by following equations:

$$E = hv = \frac{1240}{\lambda} \quad (1)$$

and

$$\alpha = \frac{4\pi(Absorbance)}{\lambda} \quad (2)$$

The relation among E and α can be given as:

$$(\alpha hv) = B(hv - H_g)^{1/2} \quad (3)$$

Equations (1)–(3) were used to draw Tauc's plot for pure tin oxide nanoparticles. From Tauc's plot, the observed band gaps of pure tin oxide nanoparticles and SGCN were found at 3.42 eV and 2.78 eV, respectively. These values were very close to the reported values [60,61]. The results showed a remarkable reduction in the band gap of Co-SnO₂, which was obtained at 3.21 eV. Similarly, the estimated band gap for 7% Co-SnO₂/50% SGCN was noted at 2.59 eV. These results showed a remarkable reduction in the band gap of nanocomposites and doped nanoparticles as compared to pure tin oxide, which played a vital role in the photocatalytic degradation of methylene blue. Figure 5b shows band gaps for SnO₂, 7% Co-SnO₂, SGCN, and 7% Co-SnO₂/50% SGCN.

3.5. Photocatalytic Study

The photocatalytic proficiency of the photocatalysts (SnO₂ and Co-SnO₂ NPs, and Co-SnO₂/50% SGCN NCs) was assessed against a model dye (MB) by checking their dye degradation capability under sunlight, employing a UV-Vis spectrophotometer with a 200–700 nm wavelength range. The UV-visible spectra exhibited that the absorbance

intensity of MB for all the doped nanoparticles decreased with increasing time, indicating an increase in the degradation of MB. At the same time, the rate of degradation of methylene blue with various concentrations of synthesized nanomaterials was determined by the following equation.

$$\text{Rate} = C/C_0$$

Figure 6b shows the photocatalytic efficiency of SnO₂ and (1, 3, 5, 7, and 9 wt.%) Co-SnO₂ NPs against MB. From Figure 6a,b, it can be seen that 7% Co-SnO₂ NPs showed the maximum degradation of MB (83% in 150 min) as compared to other fabricated samples. From Figure 6b, the plots of C/C₀ versus time for the degradation of MB in the presence of photocatalysts show that the pure SnO₂ degraded less dye than the nanoparticles of Co-SnO₂. The reason for the highest degradation by 7% Co-SnO₂ is that Co ions and oxygen states that act as electron and hole pair trapping centers introduce defect levels between the conduction and valance bands. These trapping centers reduce the recombination of electron-hole pairs and increase photocatalytic activity. However, photocatalytic activity was increased at the optimal level of cobalt doping (7%); after that, the photocatalytic activity began to decrease. When there is a high level of doping, it provides recombination centers for electron-hole pair recombination and decreases photocatalytic activity [58,62,63]. The bar graph in Figure 6c shows the final % degradation of MB dye by various Co-SnO₂ NPs after 150 min.

To make Co-SnO₂ work better as a photocatalyst, SGCN was used as a substrate to make nanocomposites of it. The catalytic performance of the produced NCs was tested under sunlight every 15 min, using the same procedure as in Section 2.7. Following the method described by Qamar et al. the photocatalysts were left in the dark until an adsorption-desorption equilibrium was reached between the dye and the NCs [64]. Nanocomposites exhibited better absorption than pure tin oxide and cobalt-doped tin oxide, which led to a higher degradation rate. From Figure 7a,b, it can be seen that the Co-SnO₂/50% SGCN nanocomposites showed the highest degradation among all the samples, and it degraded 98% of the MB dye in 120 min. The good photocatalytic activity of 7% Co-SnO₂/50% SGCN is ascribed to the formation of good heterojunction between Co-SnO₂ and SGCN, which prevents electron-hole pair recombination. The good synergetic impact between Co-SnO₂ and SGCN provides more defects in the heterostructure, which provides more sites for the dye to attach. Then the attached dye is more susceptible to degradation.

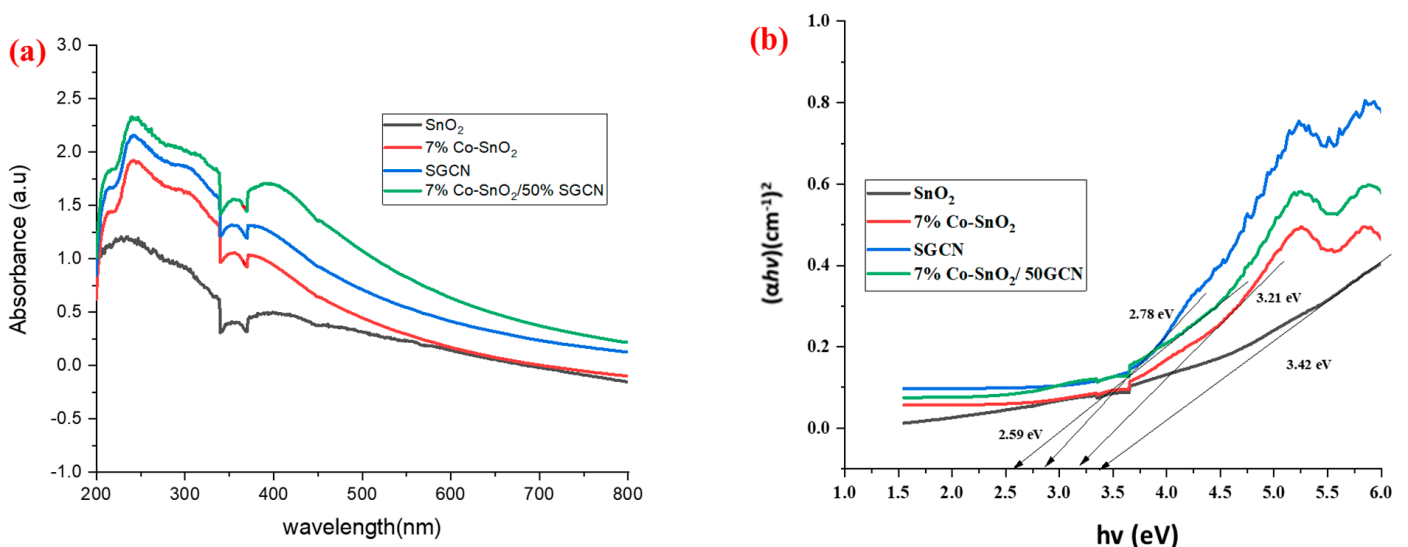


Figure 5. Absorption spectra (a) and bandgap of SnO₂, 7% Co-SnO₂, and 7% Co-SnO₂/50% SGCN (b).

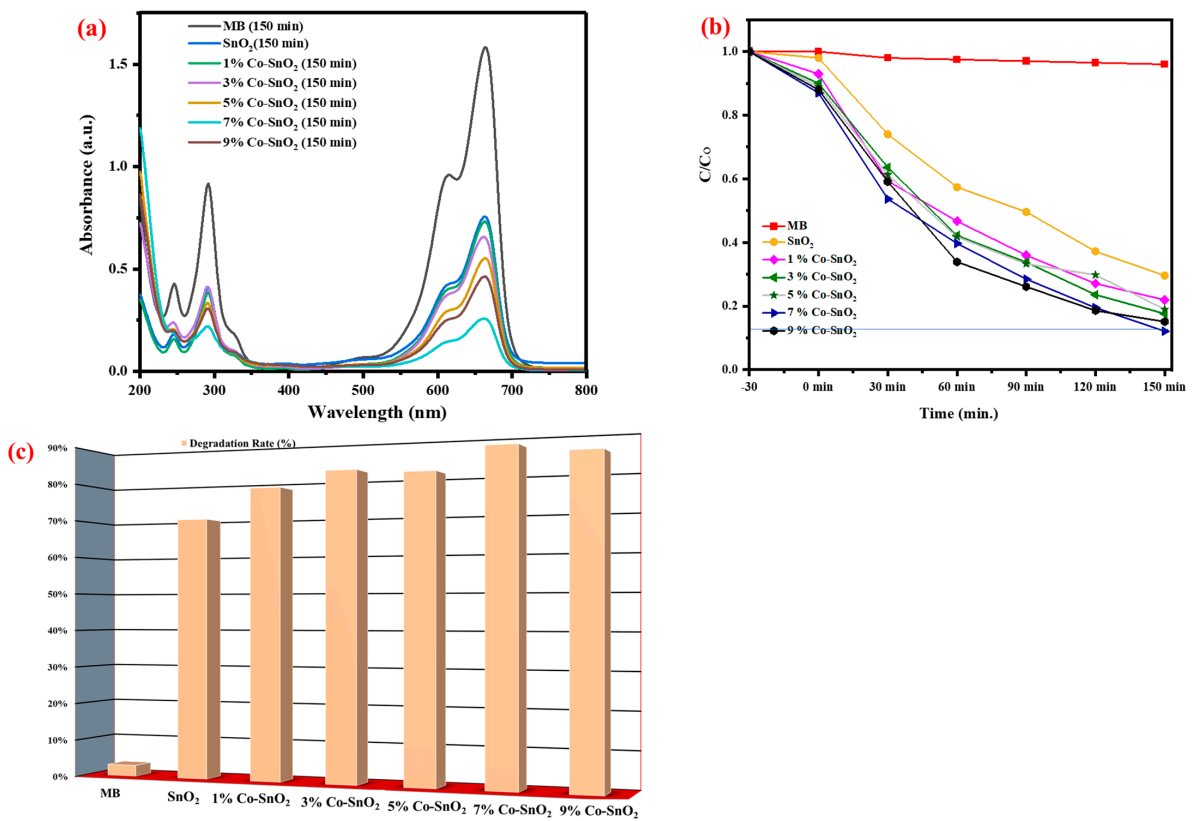


Figure 6. Degradation contours (a) Degradation rate (b) % Degradation of MB (c) by SnO₂ and Co-SnO₂ NPs.

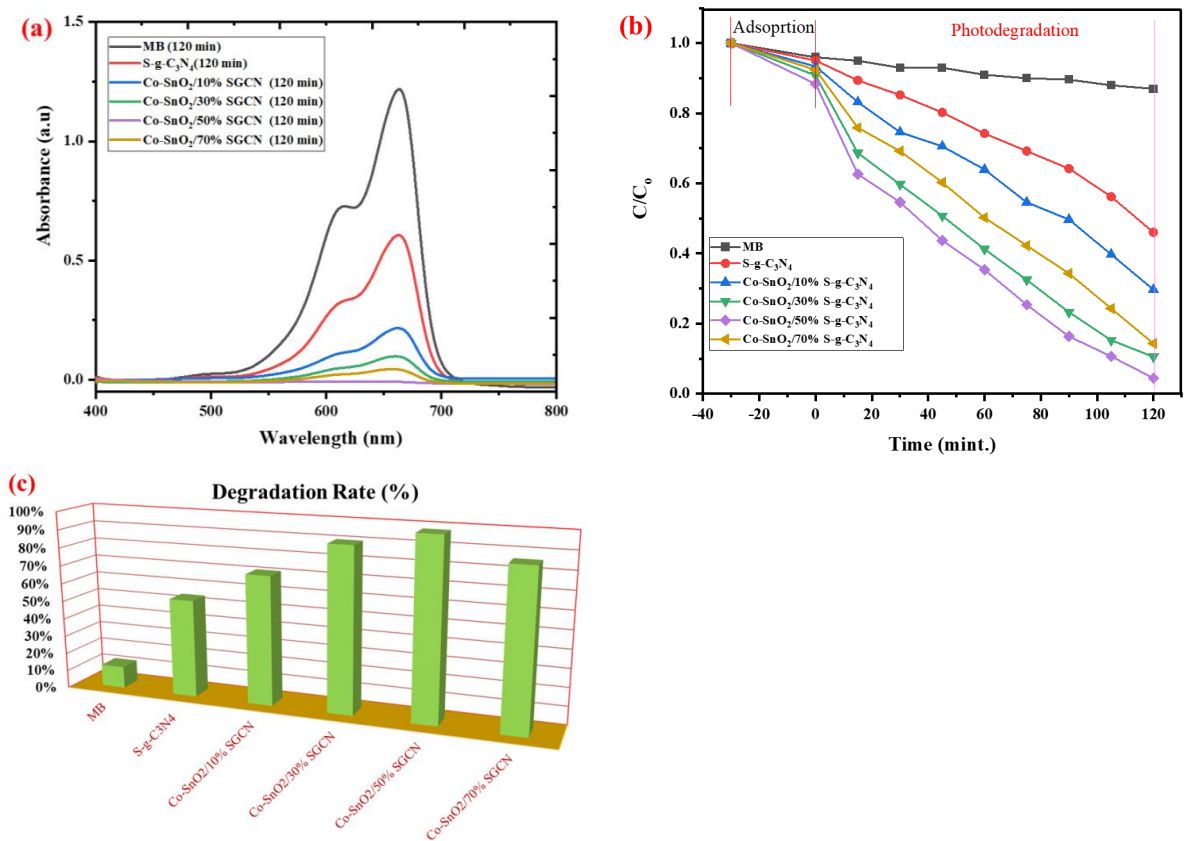


Figure 7. Degradation contours (a) Degradation rate (b) % Degradation of MB (c) by Co-SnO₂/SGCN.

Figure 7c presents the bar graph of the % degradation of MB by NCs. It is evident from the graph that the lowest degradation rate is shown by the methylene blue solution, which is kept without a photocatalyst. The methylene blue degradation rate with 7% Co-SnO₂/50% SGCN nanocomposite is faster than all other composites, as shown in Figure 8b,c. A further increase in SGCN concentrations > 50% decreases the catalytic efficiency and suppresses MB's degradation. It means that the optimum concentration of SGCN to enhance photocatalytic activity is 50%. The photocatalytic effectiveness of the 7% Co-SnO₂/50% SGCN NC is higher than that of the previously reported composites because Co-SnO₂ and SGCN successfully formed good heterojunctions [60–68]. The transport and separation of e⁻ and h⁺ in the composite may also be facilitated by cobalt atoms.

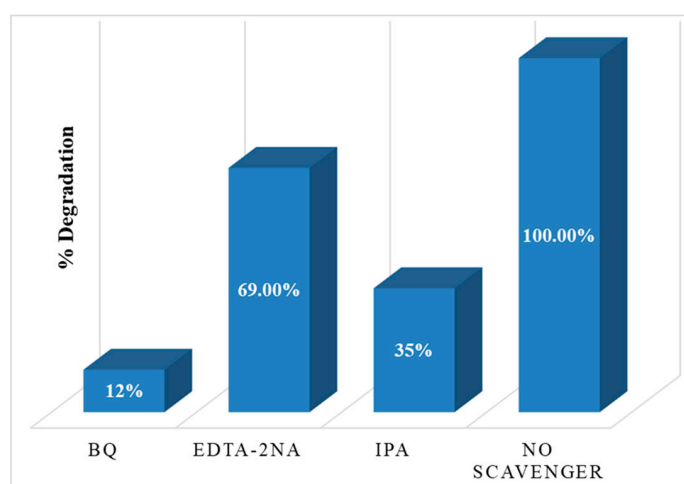


Figure 8. Effect of radical scavengers in the catalytic degradation of MB with Co-SnO₂/50% SGCN.

Superoxide radicals ($\cdot\text{O}_2^-$), hydroxyl radicals ($\cdot\text{OH}$), and photogenerated holes (h^+) are often the main active species for the degradation of organic contaminants in water. The importance of active species ($\cdot\text{OH}$, h^+ , and $\cdot\text{O}_2^-$) in the photocatalytic reaction was investigated in order to explore the photodegradation mechanism of MB by the Co-SnO₂/50% SGCN catalyst (Figure 8). Particularly, benzoquinone (BQ) was used to trap $\cdot\text{O}_2^-$, isopropanol (IPA) was used to trap $\cdot\text{OH}$, and EDTA-2Na was used to capture holes (h^+). The efficiency of MB deterioration was reduced by 88% after adding benzoquinone. However, the degradation rates of MB were only significantly reduced by 65% and 31%, respectively, by IPA and EDTA-2Na. The scavenging effect of the free radicals is given by the bar graph as shown in Figure 8. The results showed that, instead of holes (h^+), the $\cdot\text{OH}$ and $\cdot\text{O}_2^-$ are the major reactive species involved in photocatalytic dye degradation.

The MB photodegradation recycling experiment evaluated the stability of Co-SnO₂/50% SGCN NCs. The photocatalytic efficiency curve of Co-SnO₂/50% SGCN NCs against MB for five cycles under sunlight is shown in Figure 9a. In the sixth cycle, 90% of the MB is degraded, compared to 98% in the first cycle. This suggests that photocatalysis slows down less and is more stable. After five degradation experiments, the XRD showed only a slight decrease in peak intensities (Figure 9b). This experiment validates the stability of the fabricated composite. Homogeneous hybridization of SGCN layers and Co-SnO₂ NPs enhances the stability of Co-SnO₂/50% SGCN NCs. Table 3 compares the photocatalytic effectiveness of Co-SnO₂/SGCN NCs to earlier works.

Antibacterial activity was performed against gram-positive (*B. subtilis*) and gram-negative bacteria (*E. coli*). The observed ZOI without light irradiation during the antibacterial activity experiment was negligible, indicating that the substances themselves were not toxic to *E. coli* and *B. subtilis*. Table 4 shows the antibacterial activity of pure tin oxide, cobalt-doped tin oxide, and its composite with sulphur-doped graphitic carbon nitride at various concentrations i.e., at 100 ppm, 150 ppm, 200 ppm, and 250 ppm under light (LED lamp).

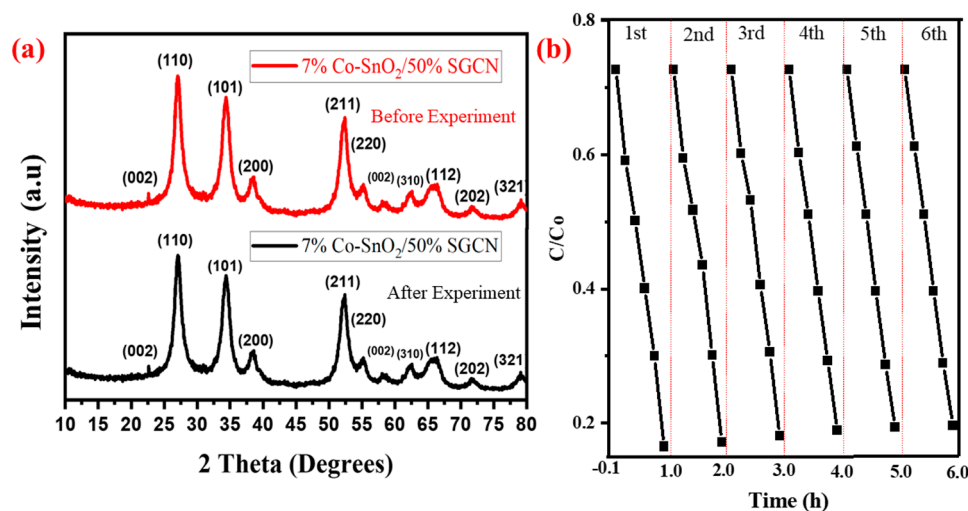


Figure 9. The stability and recyclability of the photocatalyst (a). X-ray diffraction patterns of the Co-SnO₂/50% SGCN NCs before the experiment and after the 6th cycle (b).

Table 3. Efficiency comparisons for photocatalysis of the Co-SnO₂/SGCN NCs with some previous works.

Sr. No	Photocatalyst	Contaminant	Light Source	Radiation Time (min.)	Degradation %	Ref.
1	SnO ₂	MB	Solar	180	100	[65]
2	SnO ₂ -TiO ₂	RhB	Visible	120	90	[66]
3	Co-SnO ₂	RhB	Visible	250	60	[32]
4	ZnO-SnO ₂	MB	Xe lamp	180	95	[67]
5	Zn ₂ SnO ₄ -SnO ₂	MB	UV-Visible	360	99.4	[68]
6	Fe ₂ O ₃ /SnO ₂	MB	UV	90	70	[69]
7	TiO ₂ /Ag/SnO ₂	MB	Visible	140	90	[70]
8	Co-SnO ₂ /SGCN	MB	Solar	120	98	Present Work

Table 4. Antibacterial activity against *E. coli* and *B. subtilis*.

Samples	Diameter of ZOI (mm) for Different Concentrations (ppm)							
	<i>E. coli</i>				<i>B. subtilis</i>			
	100	150	200	250	100	150	200	250
Tin oxide	-	12	15	17	-	-	11	14
7% Co-SnO ₂	19	22	25	30	16	19	21	23
7% Co-SnO ₂ /SGCN	31	34	39	42	20	24	29	31

It has been observed from the photocatalytic activity that all the prepared samples act as photocatalysts under sunlight irradiation, which degrades the dye, i.e., methylene blue, by the formation of reactive oxygen species (ROS). The amount of ROS formed is light-dependent; as the production of ROS increases under the sun, the antibacterial activity of nanoparticles and nanocomposites also increases significantly [70,71]. Another factor that affects the antimicrobial activity of tin oxide and its composites is the energy band gap. The lower band energy and the higher surface area provide good antibacterial results. By evaluating the results and comparing zones of inhibition, it was found that tin oxide showed no antibacterial activity at 100 ppm concentration, while at higher concentrations it showed activity against both gram-positive and gram-negative bacteria. At all concentrations, the nanocomposite demonstrated good antibacterial activity against gram-negative (*E. coli*) (Figure 10a) and gram-positive (*B. subtilis*) (Figure 10b) bacterial strains. The lowest antibacterial activity was shown by tin oxide, cobalt-doped tin oxide also showed good results.

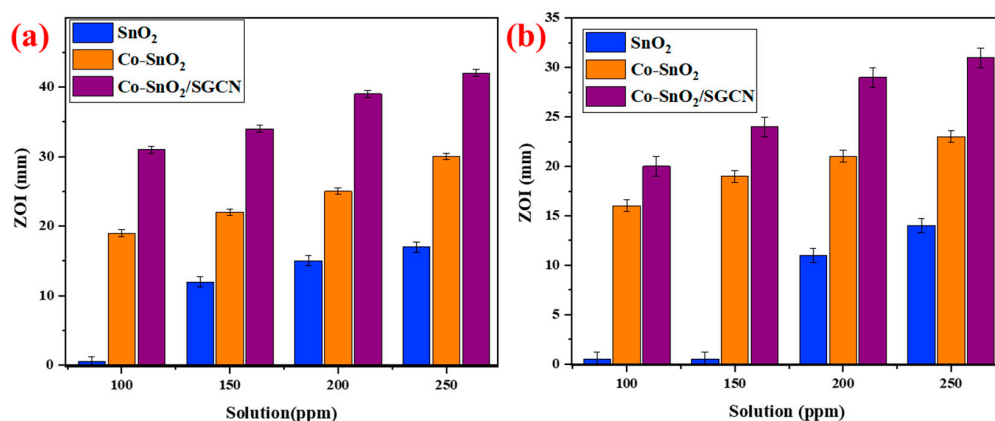


Figure 10. ZOI diameter of SnO₂, Co-SnO₂ and 7% Co-SnO₂/50% SGCN against *E. coli*. (a) and *B. subtilis* (b).

3.6. Photocatalytic Degradation Mechanism

As anticipated by a schematic diagram, the creation of e^-/h^+ pairs in the photocatalysts may be responsible for the rapid degradation of methylene blue and the antibacterial action of photocatalysts (Figure 11). When Co-SnO₂/S-g-C₃N₄ is exposed to solar radiation, both Co-SnO₂ and S-g-C₃N₄ are energized and e^-/h^+ pairs are photogenerated on their conduction band (CB) and valence band (VB), respectively [71,72]. Since the conduction band (CB) of Co-SnO₂ had a lower potential than the CB of S-g-C₃N₄ (−1.12 eV) based on the energy level of CB/VB, the photo-induced electrons moved between the two bands with ease. Additionally, Co-SnO₂ may absorb the holes that were made in the VB of S-g-C₃N₄ [61]. The presence of Co atoms in the hybrid composite not only reduced the value of E_g but also facilitated the transfer of electrons from S-g-C₃N₄ to Co-SnO₂. Therefore, doping might considerably reduce the likelihood of charge recombination by raising the separation of photoexcited e^-/h^+ pairs. Reactive oxygen species (ROS) are created when the photogenerated e^-/h^+ interact with oxygen and water molecules that are on the photocatalyst's surface. The produced radicals then degrade MB and kill bacteria in an oxidative manner to degrade MB [72].

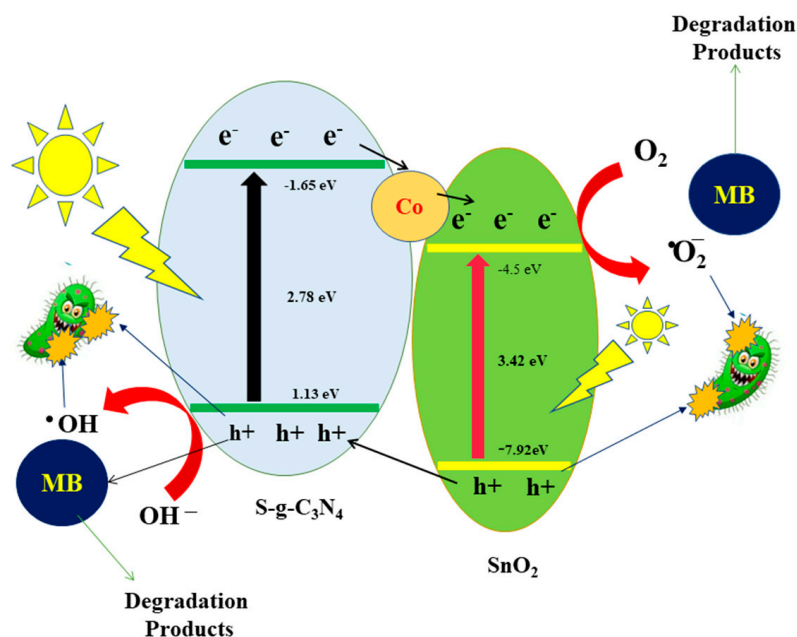


Figure 11. An illustration of the catalytic degradation mechanism of MB under sunlight over the Co-SnO₂/S-g-C₃N₄ NCs.

4. Conclusions

Doping cobalt into SnO₂ nanostructures and then integrating it into sulfur-doped graphitic carbon nitride has been found to be an excellent way to increase catalytic efficiency under solar light. The dye degradation results of a series of Co-SnO₂ samples were compared via UV-visible spectroscopy, and it was found that by increasing the concentration of cobalt in SnO₂ nanoparticles, the rate of degradation was enhanced regularly. The band gap of SnO₂ narrowed from 3.42 eV to 3.21 eV by Co-doping of SnO₂ nanoparticles (7 wt.%) In order to achieve the highest degradation in a short time period, the 7% Co-SnO₂ NPs with the best catalytic efficiency were integrated into different concentrations of S-g-C₃N₄. The NCs containing the 50%SGCN showed higher photocatalytic activity. The nanomaterials were tested to see how efficiently they killed both gram-positive and gram-negative bacteria. The 7% Co-SnO₂/50% SGCN NCs demonstrated higher photocatalytic and antibacterial activity. Ultimately, the findings of this research give us a new understanding of how to create efficient photocatalysts for bactericidal and organic pollutant degradation applications.

Author Contributions: Conceptualization, M.J.; methodology, S.I.; software, S.K.A.; validation, I.A.A., M.S.K. and N.A.M.; formal analysis, M.S.; investigation, M.A.Q. and S.I.; resources, H.A.; data curation, M.J.; writing—original draft preparation, S.I. and M.A.Q.; writing—review and editing, M.S. and N.A.M.; visualization, T.M.A.; supervision, M.J.; project administration, I.A.A.; funding acquisition, A.B. All authors have read and agreed to the published version of the manuscript.

Funding: The current work was assisted financially by the Dean of Science and Research at King Khalid University via the General Research Project: Grant no. (R.G.P.1/320/43). This research work was supported by Princess Nourah bint Abdulrahman University Researchers Supporting Project number (PNURSP2023R230), Princess Nourah bint Abdulrahman University, Riyadh, Saudi Arabia.

Data Availability Statement: Not Applicable.

Acknowledgments: The authors are grateful to the Dean of Science and Research at King Khalid University for making financial support available. This research work was funded by Princess Nourah bint Abdulrahman University Researchers Supporting Project number (PNURSP2023R230), Princess Nourah bint Abdulrahman University, Riyadh, Saudi Arabia.

Conflicts of Interest: The authors declare no conflict of interest.

References

1. Qamar, M.A.; Shahid, S.; Javed, M.; Shariq, M.; Fadhali, M.M.; Madkhali, O.; Ali, S.K.; Syed, I.S.; Awaji, M.Y.; Shakir Khan, M.; et al. Accelerated Decoloration of Organic Dyes from Wastewater Using Ternary Metal/g-C₃N₄/ZnO Nanocomposites: An Investigation of Impact of g-C₃N₄ Concentration and Ni and Mn Doping. *Catalysts* **2022**, *12*, 1388. [[CrossRef](#)]
2. Rasalingam, S.; Wu, C.-M.; Koodali, R.T. Modulation of Pore Sizes of Titanium Dioxide Photocatalysts by a Facile Template Free Hydrothermal Synthesis Method: Implications for Photocatalytic Degradation of Rhodamine B. *ACS Appl. Mater. Interfaces* **2015**, *7*, 4368–4380. [[CrossRef](#)] [[PubMed](#)]
3. Di Mauro, A.; Cantarella, M.; Nicotra, G.; Pellegrino, G.; Gulino, A.; Brundo, M.V.; Privitera, V.; Impellizzeri, G. Novel synthesis of ZnO/PMMA nanocomposites for photocatalytic applications. *Sci. Rep.* **2017**, *7*, 40895. [[CrossRef](#)] [[PubMed](#)]
4. Mulushewa, Z.; Dinbore, W.T.; Ayele, Y. Removal of methylene blue from textile waste water using kaolin and zeolite-x synthesized from Ethiopian kaolin. *Environ. Anal. Health Toxicol.* **2021**, *36*, e2021007. [[CrossRef](#)] [[PubMed](#)]
5. Uddin, M.J.; Ampiw, R.E.; Lee, W.J.C. Adsorptive removal of dyes from wastewater using a metal-organic framework: A review. *Chemosphere* **2021**, *284*, 131314. [[CrossRef](#)] [[PubMed](#)]
6. Elango, G.; Roopan, S.M.; Biology, P.B. Efficacy of SnO₂ nanoparticles toward photocatalytic degradation of methylene blue dye. *J. Photochem. Photobiol. B Biol.* **2016**, *155*, 34–38. [[CrossRef](#)] [[PubMed](#)]
7. Qamar, M.A.; Javed, M.; Shahid, S.; Shariq, M.; Fadhali, M.M.; Ali, S.K.; Khan, M.S. Synthesis and applications of graphitic carbon nitride (g-C₃N₄) based membranes for wastewater treatment: A critical review. *Heliyon* **2023**, *9*, e12685. [[CrossRef](#)]
8. Alinsafi, A.; Evenou, F.; Abdulkarim, E.; Pons, M.-N.; Zahraa, O.; Benhammou, A.; Yaacoubi, A.; Nejmeddine, A.J.D.; Pigments. Treatment of textile industry wastewater by supported photocatalysis. *Dye. Pigment.* **2007**, *74*, 439–445. [[CrossRef](#)]
9. Schwarzenbach, R.P.; Egli, T.; Hofstetter, T.B.; Von Gunten, U.; Wehrli, B. Global water pollution and human health. *Annu. Rev. Environ. Resour.* **2010**, *35*, 109–136. [[CrossRef](#)]
10. Rao, C.; Zhou, L.; Pan, Y.; Lu, C.; Qin, X.; Sakiyama, H.; Muddassir, M.; Liu, J. The extra-large calixarene-based MOFs-derived hierarchical composites for photocatalysis of dye: Facile syntheses and contribution of carbon species. *J. Alloys Compd.* **2022**, *897*, 163178. [[CrossRef](#)]

11. Husain, S.; Alam, M.M.; Imran, M.; Ali, M.A.; Ahamad, T.; Haidyrah, A.S.; Alotaibi, S.M.R.; Naik, M.-u.-d.; Shariq, M. A facile low-cost scheme for highly photoactive Fe₃O₄-MWCNTs nanocomposite material for degradation of methylene blue. *Alex. Eng. J.* **2022**, *61*, 9107–9117. [[CrossRef](#)]
12. Qamar, M.A.; Shahid, S.; Javed, M.; Sher, M.; Iqbal, S.; Bahadur, A.; Li, D. Fabricated novel g-C₃N₄/Mn doped ZnO nanocomposite as highly active photocatalyst for the disinfection of pathogens and degradation of the organic pollutants from wastewater under sunlight radiations. *Colloids Surf. A Physicochem. Eng. Asp.* **2021**, *611*, 125863. [[CrossRef](#)]
13. Imran, M.; Abutaleb, A.; Ali, M.A.; Ahamad, T.; Ansari, A.R.; Shariq, M.; Lolla, D.; Khan, A. UV light enabled photocatalytic activity of α-Fe₂O₃ nanoparticles synthesized via phase transformation. *Mater. Lett.* **2022**, *258*, 126748. [[CrossRef](#)]
14. Khan, I.; Saeed, K.; Zekker, I.; Zhang, B.; Hendi, A.H.; Ahmad, A.; Ahmad, S.; Zada, N.; Ahmad, H.; Shah, L.A.; et al. Review on Methylene Blue: Its Properties, Uses, Toxicity and Photodegradation. *Water* **2022**, *14*, 242. [[CrossRef](#)]
15. Nidheesh, P.V.; Couras, C.; Karim, A.V.; Nadais, H.J. A review of integrated advanced oxidation processes and biological processes for organic pollutant removal. *Chem. Eng. Commun.* **2022**, *209*, 390–432. [[CrossRef](#)]
16. Ganiyu, S.O.; Martínez-Huitle, C.A.; Oturan, M.A. Electrochemical advanced oxidation processes for wastewater treatment: Advances in formation and detection of reactive species and mechanisms. *Curr. Opin. Electrochem.* **2021**, *27*, 100678. [[CrossRef](#)]
17. Zahid, A.; Mukhtar, Z.; Qamar, M.A.; Shahid, S.; Ali, S.K.; Shariq, M.; Alathlawi, H.J.; Hasan, M.A.; Khan, M.S.; Islam, S.; et al. Synthesis of Mn-Doped ZnO Nanoparticles and Their Application in the Transesterification of Castor Oil. *Catalysts* **2023**, *13*, 105. [[CrossRef](#)]
18. Ikram, M.; Khan, M.; Raza, A.; Imran, M.; Ul-Hamid, A.; Ali, S. Outstanding performance of silver-decorated MoS₂ nanopetals used as nanocatalyst for synthetic dye degradation. *Phys. E Low-Dimens. Syst. Nanostruct.* **2020**, *124*, 114246. [[CrossRef](#)]
19. Ikram, M.; Raza, A.; Imran, M.; Ul-Hamid, A.; Shahbaz, A.; Ali, S.J. Hydrothermal synthesis of silver decorated reduced graphene oxide (rGO) nanoflakes with effective photocatalytic activity for wastewater treatment. *Nanoscale Res. Lett.* **2020**, *15*, 95.
20. Rafiq, A.; Ikram, M.; Ali, S.; Niaz, F.; Khan, M.; Khan, Q.; Maqbool, M.J. Photocatalytic degradation of dyes using semiconductor photocatalysts to clean industrial water pollution. *J. Ind. Eng. Chem.* **2021**, *97*, 111–128. [[CrossRef](#)]
21. Furka, D.; Furka, S.; Naftaly, M.; Rakovský, E.; Čaplovičová, M.; Janek, M.J. ZnO nanoparticles as photodegradation agent controlled by morphology and boron doping. *Catal. Sci. Technol.* **2021**, *11*, 2167–2185. [[CrossRef](#)]
22. Zhao, Y.; Li, L.; Ding, B.; Wang, X.-G.; Liu, Z.-Y.; Yang, E.-C.; Zhao, X.-J.J. Encapsulated anion-dominated photocatalytic and adsorption performances for organic dye degradation and oxoanion pollutant capture over cationic Cu (I)-organic framework semiconductors. *Dalton Trans.* **2021**, *50*, 197–207. [[CrossRef](#)] [[PubMed](#)]
23. Zheng, M.; Chen, J.; Zhang, L.; Cheng, Y.; Lu, C.; Liu, Y.; Singh, A.; Trivedi, M.; Kumar, A.; Liu, J. Metal Organic Framework as an Efficient Adsorbent for Drugs from Wastewater. *Mater. Today Commun.* **2022**, *31*, 103514. [[CrossRef](#)]
24. Alyani, S.J.; Pirbazari, A.E.; Khalilsaraei, F.E.; Kolur, N.A.; Gilani, N.J. Growing Co-doped TiO₂ nanosheets on reduced graphene oxide for efficient photocatalytic removal of tetracycline antibiotic from aqueous solution and modeling the process by artificial neural network. *J. Alloys Compd.* **2019**, *799*, 169–182. [[CrossRef](#)]
25. Mohd Kaus, N.H.; Rithwan, A.F.; Adnan, R.; Ibrahim, M.L.; Thongmee, S.; Mohd Yusoff, S.F. Effective strategies, mechanisms, and photocatalytic efficiency of semiconductor nanomaterials incorporating rGO for environmental contaminant degradation. *Catalysts* **2021**, *11*, 302. [[CrossRef](#)]
26. Al Kausor, M.; Chakraborty, D. Graphene oxide based semiconductor photocatalysts for degradation of organic dye in waste water: A review on fabrication, performance enhancement and challenges. *Inorg. Chem. Commun.* **2021**, *129*, 108630. [[CrossRef](#)]
27. Zhang, L.-S.; Jiang, L.-Y.; Yan, H.-J.; Wang, W.D.; Wang, W.; Song, W.-G.; Guo, Y.-G.; Wan, L.-J. Mono dispersed SnO₂ nanoparticles on both sides of single layer graphene sheets as anode materials in Li-ion batteries. *J. Mater. Chem.* **2010**, *20*, 5462–5467. [[CrossRef](#)]
28. Basnet, P.; Samanta, D.; Chanu, T.I.; Chatterjee, S.J. Visible light facilitated degradation of alternate dye solutions by highly reusable Mn-ZnO nano-photocatalyst. *J. Alloys Compd.* **2021**, *867*, 158870. [[CrossRef](#)]
29. Singh, J.; Juneja, S.; Soni, R.; Bhattacharya, J. Sunlight mediated enhanced photocatalytic activity of TiO₂ nanoparticles functionalized CuO-Cu₂O nanorods for removal of methylene blue and oxytetracycline hydrochloride. *J. Colloid Interface Sci.* **2021**, *590*, 60–71. [[CrossRef](#)]
30. Rosaline, D.R.; Suganthi, A.; Vinodhkumar, G.; Inbanathan, S.; Umar, A.; Ameen, S.; Akhtar, M.S.; LuizFoletto, E.J. Enhanced sunlight-driven photocatalytic activity of SnO₂-Sb₂O₃ composite towards emerging contaminant degradation in water. *J. Alloys Compd.* **2022**, *897*, 162935. [[CrossRef](#)]
31. Qin, N.; Pan, A.; Yuan, J.; Ke, F.; Wu, X.; Zhu, J.; Liu, J.; Zhu, J. One-Step Construction of a Hollow Au@ Bimetal–Organic Framework Core–Shell Catalytic Nanoreactor for Selective Alcohol Oxidation Reaction. *ACS Appl. Mater. Interfaces* **2021**, *13*, 12463–12471. [[CrossRef](#)] [[PubMed](#)]
32. Toloman, D.; Popa, A.; Stefan, M.; Silipas, T.D.; Suci, R.C.; Barbu-Tudoran, L.; Pana, O. Enhanced photocatalytic activity of Co doped SnO₂ nanoparticles by controlling the oxygen vacancy states. *Opt. Mater.* **2020**, *110*, 110472. [[CrossRef](#)]
33. Batzill, M.; Diebold, U. The surface and materials science of tin oxide. *Prog. Surf. Sci.* **2005**, *79*, 47–154. [[CrossRef](#)]
34. Parthibavarman, M.; Vallalperuman, K.; Sathishkumar, S.; Durairaj, M.; Thavamani, K. A novel microwave synthesis of nanocrystalline SnO₂ and its structural optical and dielectric properties. *J. Mater. Sci. Mater. Electron.* **2014**, *25*, 730–735. [[CrossRef](#)]
35. Patil, G.E.; Kajale, D.; Chavan, D.; Pawar, N.; Ahire, P.; Shinde, S.; Gaikwad, V.; Jain, G. Synthesis, characterization and gas sensing performance of SnO₂ thin films prepared by spray pyrolysis. *Bull. Mater. Sci.* **2011**, *34*, 1–9. [[CrossRef](#)]

36. Buniyamin, I.; Akhir, R.M.; Asli, N.A.; Khusaimi, Z.; Mahmood, M.R. Biosynthesis of SnO₂ nanoparticles by aqueous leaves extract of *Aquilaria malaccensis* (agarwood). *IOP Conf. Ser. Mater. Sci. Eng.* **2021**, *1092*, 012070. [[CrossRef](#)]
37. Sharma, S.; Vats, M.; Sharma, J.; Chhabra, A.; Kumar, R.R.; Chuang, C.-H. Synthesis, Characterization and Photocatalytic Activity of Tin Oxide Nanocrystals. *Curr. Nanosci.* **2021**, *17*, 612–619. [[CrossRef](#)]
38. Ahmadabad, L.E.; Kalantari, F.S.; Liu, H.; Hasan, A.; Gamasaee, N.A.; Edis, Z.; Attar, F.; Ale-Ebrahim, M.; Rouhollah, F.; Babadaei, M.M.N.; et al. Hydrothermal method-based synthesized tin oxide nanoparticles: Albumin binding and antiproliferative activity against K562 cells. *Mater. Sci. Eng. C* **2021**, *119*, 111649. [[CrossRef](#)]
39. Mishra, S.R.; Ahmaruzzaman, M.J. Tin oxide based nanostructured materials: Synthesis and potential applications. *Nanoscale* **2021**, *14*, 1566–1605. [[CrossRef](#)]
40. Shahzad, N.; Ali, N.; Shahid, A.; Khan, S.; Alrobei, H. Synthesis of tin oxide nanoparticles in order to study its properties. *Dig. J. Nanomater. Biostruct.* **2021**, *16*, 41–49. [[CrossRef](#)]
41. Vaseghi, Z.; Nematollahzadeh, A. Nanomaterials: Types, Synthesis, and Characterization. In *Green Synthesis of Nanomaterials for Bioenergy Applications*; John Wiley & Sons: Hoboken, NJ, USA, 2020; pp. 23–82.
42. Mani, R.; Vivekanandan, K.; Vallalperuman, K. Synthesis of pure and cobalt (Co) doped SnO₂ nanoparticles and its structural, optical and photocatalytic properties. *J. Mater. Sci. Mater. Electron.* **2017**, *28*, 4396–4402. [[CrossRef](#)]
43. Kolahalalam, L.A.; Viswanath, I.K.; Diwakar, B.S.; Govindh, B.; Reddy, V.; Murthy, Y. Review on nanomaterials: Synthesis and applications. *Mater. Today Proc.* **2019**, *18*, 2182–2190. [[CrossRef](#)]
44. Rane, A.V.; Kanny, K.; Abitha, V.; Thomas, S. Methods for synthesis of nanoparticles and fabrication of nanocomposites. In *Synthesis of Inorganic Nanomaterials*; Elsevier: Amsterdam, The Netherlands, 2018; pp. 121–139.
45. Abid, N.; Khan, A.M.; Shujait, S.; Chaudhary, K.; Ikram, M.; Imran, M.; Haider, J.; Khan, M.; Khan, Q.; Maqbool, M.; et al. Synthesis of nanomaterials using various top-down and bottom-up approaches, influencing factors, advantages, and disadvantages: A review. *Adv. Colloid Interface Sci.* **2021**, *300*, 102597. [[CrossRef](#)] [[PubMed](#)]
46. Kim, S.P.; Choi, M.Y.; Choi, H.C. Photocatalytic activity of SnO₂ nanoparticles in methylene blue degradation. *Mater. Res. Bull.* **2016**, *74*, 85–89. [[CrossRef](#)]
47. Tazikeh, S.; Akbari, A.; Talebi, A.; Talebi, E. Synthesis and characterization of tin oxide nanoparticles via the Co-precipitation method. *Mater. Sci.* **2014**, *32*, 98–101. [[CrossRef](#)]
48. Chandran, D.; Nair, L.S.; Balachandran, S.; Babu, K.R.; Deepa, M.J. Structural, optical, photocatalytic, and antimicrobial activities of cobalt-doped tin oxide nanoparticles. *J. Sol-Gel Sci. Technol.* **2015**, *76*, 582–591. [[CrossRef](#)]
49. Pan, Y.; Rao, C.; Tan, X.; Ling, Y.; Singh, A.; Kumar, A.; Li, B.; Liu, J. Cobalt-seamed C-methylpyrogallol [4] arene nanocapsules-derived magnetic carbon cubes as advanced adsorbent toward drug contaminant removal. *Chem. Eng. J.* **2022**, *433*, 133857. [[CrossRef](#)]
50. Entradas, T.; Cabrita, J.; Dalui, S.; Nunes, M.; Monteiro, O.; Silvestre, A.J. Synthesis of sub-5 nm Co-doped SnO₂ nanoparticles and their structural, microstructural, optical and photocatalytic properties. *Mater. Chem. Phys.* **2014**, *147*, 563–571. [[CrossRef](#)]
51. Rashad, M.M.; Ismail, A.A.; Osama, I.; Ibrahim, I.A.; Kandil, A.H.T. Decomposition of Methylene Blue on Transition Metals Doped SnO₂ Nanoparticles. *CLEAN–Soil Air Water* **2014**, *42*, 657–663. [[CrossRef](#)]
52. Xu, Q.; Zhang, L.; Cheng, B.; Fan, J.; Yu, J.J.C. S-scheme heterojunction photocatalyst. *Chem* **2020**, *6*, 1543–1559. [[CrossRef](#)]
53. Wageh, S.; Al-Ghamdi, A.A.; Jafer, R.; Li, X.; Zhang, P. A new heterojunction in photocatalysis: S-scheme heterojunction. *Chin. J. Catal.* **2021**, *42*, 667. [[CrossRef](#)]
54. Kim, T.; Parale, V.G.; Jung, H.-N.-R.; Kim, Y.; Driss, Z.; Driss, D.; Bouabidi, A.; Euchy, S.; Park, H.-H. Facile synthesis of SnO₂ aerogel/reduced graphene oxide nanocomposites via in situ annealing for the photocatalytic degradation of methyl orange. *Nanomaterials* **2019**, *9*, 358. [[CrossRef](#)] [[PubMed](#)]
55. Liang, Y.; Li, S.; Du, M.J.C.; Science, P. Synthesis of polymer/rGO/SnO₂ hierarchical structure and its photodegradation of organic pollutants. *Colloid Polym. Sci.* **2015**, *293*, 3499–3504. [[CrossRef](#)]
56. Rajput, R.B.; Jamble, S.N.; Kale, R.B.J. A review on TiO₂/SnO₂ heterostructures as a photocatalyst for the degradation of dyes and organic pollutants. *J. Environ. Manag.* **2022**, *307*, 114533. [[CrossRef](#)] [[PubMed](#)]
57. Ali, G.; Zaidi, S.J.A.; Basit, M.A.; Park, T.J. Synergetic performance of systematically designed g-C₃N₄/rGO/SnO₂ nanocomposite for photodegradation of Rhodamine-B dye. *Appl. Surf. Sci.* **2021**, *570*, 151140. [[CrossRef](#)]
58. Qamar, M.A.; Shahid, S.; Khan, S.A.; Zaman, S.; Sarwar, M.N. Synthesis characterization, optical and antibacterial studies of Co-doped SnO₂ nanoparticles. *Dig. J. Nanomater. Biostruct.* **2017**, *12*, 1127–1135.
59. Siddiqui, M.A.; Siddiqui, M.A.; Chandel, V.S.; Shariq, M.; Azam, A. FTIR and dielectric studies of nickel doped potassium hexa-titanate (K₂Ti₆O₁₃) fine ceramics. *J. Mater. Sci. Mater. Electron.* **2013**, *24*, 4725–4731. [[CrossRef](#)]
60. Taqiullah, S.M.; Alshahrani, T.; Shariq, M.; Hakami, J.; Ahmad, N.; Alshehri, A.M.; Chaudhary, A.A.; Khan, M.S.; Shinde, S.M.; Slimani, Y.; et al. Utilization of infrared, Raman spectroscopy for structural analysis of alkali boro-germanate glasses. *J. Taibah Univ. Sci.* **2022**, *16*, 820–827. [[CrossRef](#)]
61. Sher, M.; Javed, M.; Shahid, S.; Iqbal, S.; Qamar, M.A.; Bahadur, A.; Qayyum, M.A. The controlled synthesis of gC₃N₄/Cd-doped ZnO nanocomposites as potential photocatalysts for the disinfection and degradation of organic pollutants under visible light irradiation. *RSC Adv.* **2021**, *11*, 2025–2039. [[CrossRef](#)]
62. Sowjanya, M.; Shariq, M.; Alajlani, Y.; Pamu, D.; Chowdhruy, R.; Jayaganthan, R.; Florence, S.; Haider, M. Effect of Ar: O₂ gas atmosphere on optical properties of Y₂O₃-doped ZnO thin films by RF sputtering. *EPL* **2020**, *129*, 34003. [[CrossRef](#)]

63. Ali, S.M.; Hussain, S.T.; Bakar, S.A.; Muhammad, J.; ur Rehman, N. Effect of doping on the structural and optical properties of SnO₂ thin films fabricated by aerosol assisted chemical vapor deposition. *Proc. J. Phys. Conf. Ser.* **2013**, *439*, 012013. [[CrossRef](#)]
64. Qamar, M.A.; Javed, M.; Shahid, S.; Sher, M. Fabrication of g-C₃N₄/transition metal (Fe, Co, Ni, Mn and Cr)-doped ZnO ternary composites: Excellent visible light active photocatalysts for the degradation of organic pollutants from wastewater. *Mater. Res. Bull.* **2022**, *147*, 111630. [[CrossRef](#)]
65. Luque, P.; Garrafa-Gálvez, H.; Nava, O.; Olivas, A.; Martínez-Rosas, M.; Vilchis-Nestor, A.; Villegas-Fuentes, A.; Chinchillas-Chinchillas, M. Efficient sunlight and UV photocatalytic degradation of Methyl Orange, Methylene Blue and Rhodamine B, using Citrus × paradisi synthesized SnO₂ semiconductor nanoparticles. *Ceram. Int.* **2021**, *47*, 23861–23874. [[CrossRef](#)]
66. Toloman, D.; Pana, O.; Stefan, M.; Popa, A.; Leostean, C.; Macavei, S.; Silipas, D.; Perhaita, I.; Lazar, M.D.; Barbu-Tudoran, L. Photocatalytic activity of SnO₂-TiO₂ composite nanoparticles modified with PVP. *J. Colloid Interface Sci.* **2019**, *542*, 296–307. [[CrossRef](#)]
67. Upadhaya, D.; Kumar, P.; Purkayastha, D.D. Tuning the wettability and photocatalytic efficiency of heterostructure ZnO-SnO₂ composite films with annealing temperature. *Mater. Sci. Semicond. Process.* **2019**, *95*, 28–34. [[CrossRef](#)]
68. Junploy, P.; Phuruangrat, A.; Plubphon, N.; Thongtem, S.; Thongtem, T. Photocatalytic degradation of methylene blue by Zn₂SnO₄-SnO₂ system under UV visible radiation. *Mater. Sci. Semicond. Process.* **2017**, *66*, 56–61. [[CrossRef](#)]
69. Lei, R.; Ni, H.; Chen, R.; Zhang, B.; Zhan, W.; Li, Y. Growth of Fe₂O₃/SnO₂ nanobelt arrays on iron foil for efficient photocatalytic degradation of methylene blue. *Chem. Phys. Lett.* **2017**, *673*, 1–6. [[CrossRef](#)]
70. Zhang, Z.; Ma, Y.; Bu, X.; Wu, Q.; Hang, Z.; Dong, Z.; Wu, X. Facile one-step synthesis of TiO₂/Ag/SnO₂ ternary heterostructures with enhanced visible light photocatalytic activity. *Sci. Rep.* **2018**, *8*, 10532. [[CrossRef](#)]
71. Zhong, Q.; Lan, H.; Zhang, M.; Zhu, H.; Bu, M. Preparation of heterostructure g-C₃N₄/ZnO nanorods for high photocatalytic activity on different pollutants (MB, RhB, Cr (VI) and eosin). *Ceram. Int.* **2020**, *46*, 12192–12199. [[CrossRef](#)]
72. Fu, H.; Xu, T.; Zhu, S.; Zhu, Y. Photocorrosion inhibition and enhancement of photocatalytic activity for ZnO via hybridization with C60. *Environ. Sci. Technol.* **2008**, *42*, 8064–8069. [[CrossRef](#)] [[PubMed](#)]

Disclaimer/Publisher's Note: The statements, opinions and data contained in all publications are solely those of the individual author(s) and contributor(s) and not of MDPI and/or the editor(s). MDPI and/or the editor(s) disclaim responsibility for any injury to people or property resulting from any ideas, methods, instructions or products referred to in the content.